ACS AGRICULTURAL SCIENCE & TECHNOLOGY

pubs.acs.org/acsagscitech

Article

Facile Synthesis and Optimization of Graphitic Carbon Nitride Nanoparticles to Effectively Photodegrade Tetracycline under Visible Light in Water

Sheng-Eng Huang, Kok-Hou Tan, Rama Shanker Sahu, Tesfaye Abebe Geleta, Ashkan Miri, Chen-yu Lin, Yang-hsin Shih,* and Wen-Ling Chen

Cite This: https://doi.org/10.1021/acsagscitech.4c00637

Read Online

ACCESS | Metrics & More | Article Recommendations | Supporting Information

ABSTRACT: The rapid development of industry and medicine in modern society has produced a group of emerging contaminants (ECs) that are harmful to the ecosystem and difficult to remove from the environment. In this study, several graphitic carbon nitrides (GCNs) have been successfully synthesized by the calcination method, and their efficiency in the photocatalytic degradation of tetracyclines (TCs) was evaluated under the irradiation of visible light (λ = 420 nm). CNU achieved the highest TC degradation efficiency by completely degrading tetracycline within 90 min. The best degradation rate constant of 18.9×10^{-3} min^{-1} was obtained at pH 7, which is 17-fold and 1.5-fold than that at pH 3 and pH 5, respectively. Above pH 7, the degradation rate sharply rose due to the alkaline hydrolysis of TCs. The addition of common electrolytes has been shown to reduce the photocatalytic degradation rate as a result of photocatalyst aggregation. The results of EPR, scavenging tests, and LC-QTOF/MS analysis showed that the photogenerated holes and $\bullet O_2^-$ produced by CNU upon photoirradiation degrade TC into small organic molecules such as 1-tetralone and 3-formyl propanoic acid. This study demonstrated the ease of environmentally friendly GCN preparation and their potential for the removal of ECs from the environment.

KEYWORDS: *Photocatalysis, Graphitic carbon nitrides, Reactive oxygen species, Antibiotics, Water treatment*

1. INTRODUCTION

Antibiotics have been widely applied against diseases and have saved human lives over the past few decades. Tetracycline antibiotics (TCs), as one of the primary antibiotics generated and consumed globally,[1] have been extensively applied in veterinary treatment,[2] agriculture,[3] and human diseases caused by bacterial infections.[4,5] More than 10000 tons of veterinary antibiotics were consumed every year in highly developed countries, and 60%, 43%, 48%, and 59% of the consumed antibiotics were TCs and TCs-based antibiotics in China, Japan, Europe, and the United States, respectively.[1] However, humans and animals are unable to metabolize TCs and their byproducts completely. As a result, TCs may enter the environment in active forms in feces and urine. These residues remain highly hydrophilic and stable, resulting in potential hazards to human health and organisms living in aquatic and terrestrial environments.[6] Several reports have suggested that this long-term pollution may cause the resistance of microbes, chronic toxicity to the human body,[7] and other ecological risks.[8] Therefore, removing TCs from the environment has become an urgent issue. To remove TCs and their byproducts, researchers have applied various methods and techniques, such as adsorption,[9] the photo-Fenton reaction,[10] biological processes,[11] electrochemical oxidation,[12] and photocatalysis.[13] However, applying these methods may face some difficulties and drawbacks while removing TCs. For example, adsorption can translocate only the antibiotics instead of eliminating them from the environment. A large number of anions and ferrous ions generated from the Fenton process may lead to secondary pollution.[14] TCs cannot be degraded completely through microorganisms due to their resistance.[15] Abundant energy is required during the electrochemical oxidation processes.[16] In order to overcome these drawbacks, a low-cost, highly efficient, and ecofriendly method is needed to remove TCs from the environment.

Among these methods, photocatalysis has been considered a promising strategy to degrade antibiotics and other emerging contaminants because of its green, high-performing, and sustainable features of solar energy as a driving force. Numerous photocatalysts have been fabricated and studied to degrade various organic pollutants.[17−19] Although some common photocatalysts, such as TiO_2, have shown some efficiency in degrading organic compounds, the high bandgap energy (~3.2 eV) has brought limitations for real applications.[13] To use solar energy effectively, fabricating a photocatalyst with a lower bandgap energy and broader visible light response is one of the prominent strategies. Graphitic carbon nitride (g-C_3N_4, GCN) is a semiconductor photocatalyst with a suitable bandgap energy for a visible light response (~2.7

Received: October 10, 2024
Revised: January 4, 2025
Accepted: January 6, 2025

eV). Bulk GCN materials can be easily prepared by directly heating C and N-rich precursors, e.g., melamine, urea, dicyandiamide, and thiourea. Moreover, due to its low-cost, thermostable, nontoxic, and metal-free properties,[20] GCN has drawn the attention of scholars for multiple applications, including water splitting,[21] CO_2 reduction,[22] and water disinfection.[23] Especially in the field of degradation of organic pollutants, g-C_3N_4 has demonstrated significant photocatalytic potential. In detail, Jing et al. recently reported a great enhancement in BPA degradation in water over a g-C_3N_4 photocatalyst synthesized by calcinating urea with propanedioic acid in a muffle furnace;[24] Chang et al. reported that a carbon-doped g-C_3N_4 photocatalyst showed photocatalytic performance for the degradation of trihalomethanes and haloacetonitriles under visible light irradiation;[25] Hu et al. successfully fabricated a composite of 1D/2D TiO_2 nanorod/g-C_3N_4 nanosheet and applied it to degrade 93.4% of ciprofloxacin within 60 min.[26] Recently, Oluwole and Olatunji demonstrated that up to 95.9% of TC photodegradation efficiency has been achieved using needle-like SnO_2/g-C_3N_4 under visible light irradiation.[27] Another study by Quyen and co-workers used S-doped g-C_3N_4 to remove 98.7% of TC upon 30 min of solar light exposure.[28] Based on these previous studies, GCN has been proven to possess a prospective ability to eliminate organic pollutants in the water.

Thus, this research aims to synthesize several GCN photocatalysts and apply them to the removal of TC as a pollutant in water. The as-synthesized photocatalysts are employed to degrade TC under visible LED light (λ = 420 nm) irradiation and compared with one another regarding their photocatalytic activities. Moreover, this study has tested and investigated several variables and reaction conditions such as photocatalyst dosage, pollutant concentration, initial pH, and effect of ions in water. Furthermore, the electron spin resonance (ESR) technique was used to probe the reactive oxygen species (ROS) generated during irradiation to elucidate the photocatalytic mechanism. LC-QToF/MS also verified the intermediates of the TC.

2. MATERIALS AND METHODS

2.1. Chemicals. Urea (99% purity) and potassium bromate ($KBrO_3$, 99%) were acquired from Alfa Aesar; tetracycline was bought from MP Biomedicals. Sodium perchlorate (NaClO), hydrogen peroxide (H_2O_2, 30%), potassium hydroxide (KOH), sulfuric acid (H_2SO_4), and hydrochloric acid (HCl) were purchased from Merck Co. *tert*-Butyl alcohol (*t*-BuOH, 99%) was purchased from J.T. Baker, while furfuryl alcohol (FFA, 98%) and ethylenediaminetetraacetic acid disodium salt (EDTA-2Na, 99%) were obtained from Acros. L-Ascorbic acid was purchased from Sigma-Aldrich. Double distilled ultrapure water (ddW) was utilized for photocatalytic experiments, acquired from a milli-Q water system with 18.2 $\mu\Omega$/cm resistivity. All chemicals purchased and used for the synthesis, and photocatalysis experiments were of analytical grade.

2.2. Synthesis of Photocatalysts. The GCN prepared in this study was based on the widely adapted simple calcination method, in which precursors were subjected to high temperature thermal treatment in a capped crucible.[29] Melamine and urea-based GCN were synthesized to compare their physicochemical properties and photocatalytic performance. The latter was further modified with an exfoliation process and integration with graphene quantum dots (GQDs).

2.2.1. CN-B. A moderate amount of melamine was added, and the mixture was distributed evenly in a ceramic crucible. After the muffle furnace was filled with nitrogen, the crucible was placed into the furnace and calcinated at 550 °C for 4 h at 5 °C min^{-1}. After calcination, the resulting yellow powder was rinsed with ultrapure water, filtered, and dried at 80 °C overnight in an oven. The final product was labeled as CN-B and stored in a dry place.

2.2.2. CNU. Ten grams of urea were spread evenly in an alumina crucible and heated at 550 °C for 4 h with a ramp rate of 5 °C min^{-1} in a muffle furnace. The furnace was vacuumed and filled with nitrogen during calcination. When the furnace cooled to room temperature, the light-yellow product was taken out and ground into a homogeneous powder. The obtained powder was labeled CNU and stored in a dry place for further experiments.

2.2.3. CNOU. The synthesis of CN@GQD was separated into two parts. First, exfoliated GCN was synthesized by the previous report.[30] 10 g of urea, 100 mg KOH, and 3 mL H_2O_2 (30%) were mixed by ultrasonication for 4 h. The mixture was dried and calcinated at 550 °C for 4 h at 5 °C min^{-1}. The light-yellow powder obtained was rinsed, filtered, and dried. 1.0 g of the light-yellow powder was mixed and ultrasonicated with 60 mL of 2.0 M NaClO and 15 mL of 1.0 M HNO_3 for 2 h. The mixture was then transferred to Teflon-lined autoclave tubes and heated at 130 °C for 5 h. Afterward, the mixture was removed and rinsed with ultrapure water to a neutral pH. The final product was dried at 80 °C overnight and labeled as CNOU.

2.2.4. CN@GQD. GQDs were synthesized via citric acid pyrolysis. Five grams of citric acid was added into a 200 mL round-bottom flask, and heating was started for 30 min at 200 °C. The citric acid crystals melted as the temperature rose and turned into a dark yellow liquid. It was then added drop by drop into 100 mL of a 0.2 M KOH solution under continuous stirring to produce a GQD solution. This solution was purified by transferring it into a 1 kDa dialysis tubing bag. After dialysis, a fixed amount of neutralized GQD solution was added into a breaker containing 50 mL of DI water and 1.0 g of CNOU. CNOU solution was pretreated with ultrasonicated for 60 min to form a uniform suspension, followed by the addition of GQD solution and extended ultrasonication to form CN@GQD. The resulting solution was transferred into a Teflon-lined autoclave for constant heating at 120 °C for 2 h. The product was then filtrated and dried at 80 °C overnight.

2.3. Characterization. The morphology of as-synthesized CNU, CNOU, and CN@GQD was observed using a scanning electron microscope (SEM, Joel JSM-7600F). Furthermore, the crystal structures of the as-prepared photocatalysts were analyzed by using a Bruker D8 Advanced X-ray diffractometer (XRD), Ni filtered Cu-Kα radiation (λ = 1.5405 Å, at 40 mA current density and 40 kV voltage). The zeta potential of the best-performed photocatalyst was determined using a zetasizer; 1 mg of catalyst was dispensed into 10 mL of ddW (100 mg/L) and ultrasonicated to produce a homogeneous suspension. The suspension was diluted to 50 mg/L with ddW, and its pH was measured. Two mL of suspension was transferred to a capillary cell and measured with a zetasizer. The catalyst suspensions were adjusted with 10 mM of HCl or NaOH solution to the targeted pH, and their zeta potential was determined. The optical absorption of the prepared GCNs was measured using UV−visible diffuse reflectance spectroscopy (UV−vis DRS, Jasco V-670) between 200 and 800 nm. These data were used to prepare Tauc plots for the band gap determination. Photoluminescence spectroscopy (PL, Hitachi F-7000 FL spectrophotometer) was performed at an excitation wavelength, $\lambda_{excitation}$ of 330.0 nm to evaluate the charge carrier recombination rate of the as-synthesized photocatalyst.

2.4. Photocatalytic Experiments. The process of TC photodegradation was performed in a 20 mL glass tube reactor. Apart from the experiments with a different initial dosage of photocatalysts, pH, and TC concentration, all the photocatalytic activities tests were performed using a 500 mg/L photocatalysts dosage, a solution pH of 7, and 25 ppm as the TC concentration for the optimal outcome. The mixture was placed in a dark room for 30 min to reach adsorption−desorption equilibrium before irradiation. The reactor was then exposed to the single wavelength 100 W LED light source (λ = 420 nm). 0.5 mL of solution was collected at certain intervals during irradiation and filtered through a 0.22 μm filter. The sample was analyzed by the HPLC method (1200 series, Agilent, equipped UV−vis variable wavelength detector (VWD), C18 column (150 mm × 4.6

https://doi.org/10.1021/acsagscitech.4c00637
ACS Agric. Sci. Technol. XXXX, XXX, XXX−XXX

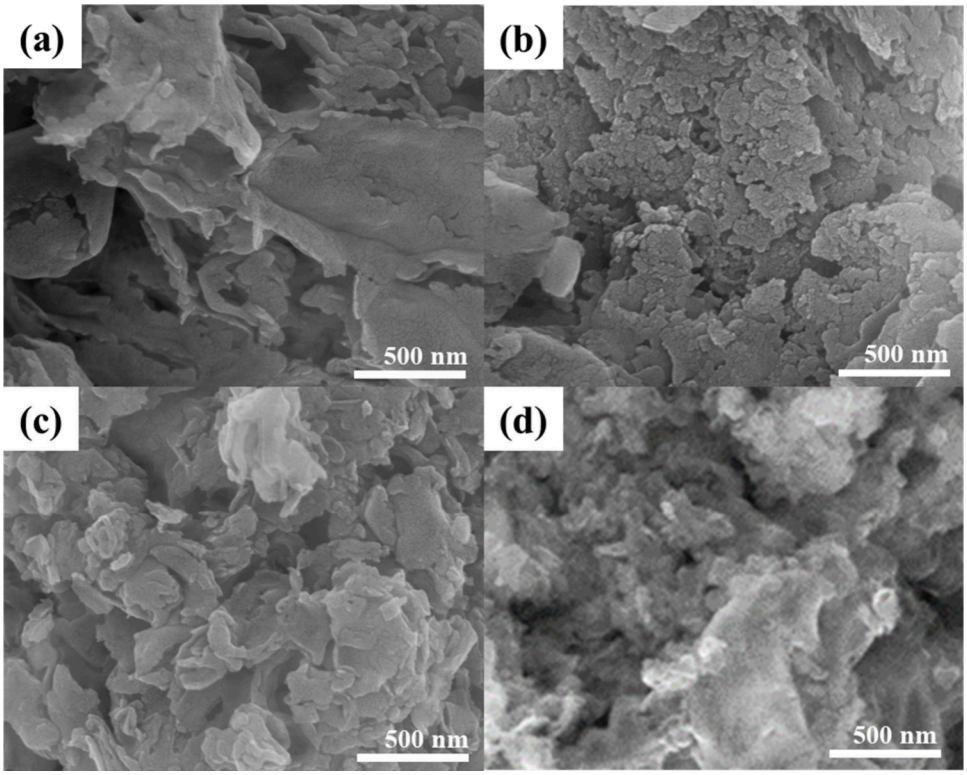

Figure 1. SEM images of (a) CN-B, (b) CNU, (c) CNOU, and (d) CN@GQD (scale bar = 500 nm).

mm, 5 μm), flow rate = 0.7 mL/min. 3% of acetic acid in a dd water and methanol (75:25; v/v) mixture was adopted as a mobile phase. Liquid chromatography−mass spectroscopy analysis was carried out on a JMS-T100LP AccuTOF LC-plus 4G mass spectrometer (JEOL, Tokyo, Japan) fitted with HR & LR-ESI (Electrospray) mode. The mass spectra of tetracycline and its degradation products were analyzed in the negative ion mode in the range of 60−500 m/z. The effect of different water chemistry was performed by DI water, tap water, and river water collected from Shihmen Reservoir, Taoyuan, Taiwan.

2.5. Scavenging Test. A 5 mM concentration of selected scavenger (*t*-BuOH, FFA, ascorbic acid, EDTA-2Na, or $KBrO_3$) was used to determine the species responsible for the GCN-catalyzed photocatalytic degradation of TC. An initial TC concentration of 25 mg/L, a catalyst dosage of 500 mg/L, and an initial pH of 7 were applied, with the experiment being carried out under visible light (420 nm) irradiation.

2.6. Measurement for Induced ROS Generation and Influence. The EPR spectra of the sample were recorded at room temperature by an EMXplus-10/12/P/L spectrometer (Bruker) using the following instrumental settings: resonance frequency: 9.82 GHz, modulation frequency: 100 kHz, modulation amplitude: 1.0 G, sweep width: 200 G, time constant: 40.96 ms, sweep time: 83.88 s, receiver gain: 30 db. As-synthesized composites were mixed with a TEMP (20 mM) solution and recorded for EPR measurement under dark and visible light. A TEMP solution was analyzed without adding any catalysts and as a blank, under similar conditions.

2.7. Evaluation of Toxicity. The toxicity of TC and its degradation intermediates was simulated using the Ecological Structure Activity Relationships (ECOSAR) tool with quantitative structure−activity relationship (QSAR) models being applied to correlate their chemical structures and biological activities. ECOSAR was utilized to estimate aquatic acute toxicity end points, including lethal concentration (LC_{50}) and effective concentration (EC_{50}), as well as chronic toxicity values (ChV) for fish, daphnia, and green algae.[31]

3. RESULTS AND DISCUSSION

3.1. Characterization of As-Prepared g-C_3N_4 Photocatalysts. The morphology of the as-prepared GCNs was observed using SEM, and its image is shown in Figure 1. It is observed that CN-B, CNOU, and CN@GQD were made up of bulk particles, while CNU consists of numerous irregular and distinct sheets. The formation of this microsheet is due to the calcination of urea at high temperatures. At high temperatures, urea undergoes extensive polymerization to form a 2D structure with irregular edges and smooth surfaces. The presence of interparticle voids gave rise to textural porosity of CNU as observed in its SEM micrograph (Figure 1b).

Figure 2 shows the XRD patterns of CNU and CN-B. Two typical GCN peaks are observed in the diffractograms of both crystalline samples. A weak peak that appears at 13.1° is due to the (100) plane of the condensed structure of tri-s-triazine units with an interplanar distance of 0.68 nm, while a strong peak at 27.4° is attributed to the stacking of conjugated aromatic systems along the (002) plane with an interplanar distance of 0.33 nm.[32] It is noted that a peak shift from 13.1° in CN-B to 13.8° in CNU indicates a decrease in d_{100}, which reflects a shorter distance between layers of microsheets. It is also revealed that the crystallite size of CNU is smaller than that of CN-B as evidenced by its broader (100) peak than that of the latter. The findings from the XRD analysis suggest that using urea as a precursor will produce GCN with a smaller crystallite size.

The light absorption ability and charge separation efficiency of GCNs were evaluated based on their UV−vis DRS spectra (Figure 3a). It was shown that CNU absorption toward near UV light is higher than that of CN-B and exfoliated but comparable to the graphene quantum dots-doped carbon nitride. The enhanced light absorption in this region can help

https://doi.org/10.1021/acsagscitech.4c00637
ACS Agric. Sci. Technol. XXXX, XXX, XXX−XXX

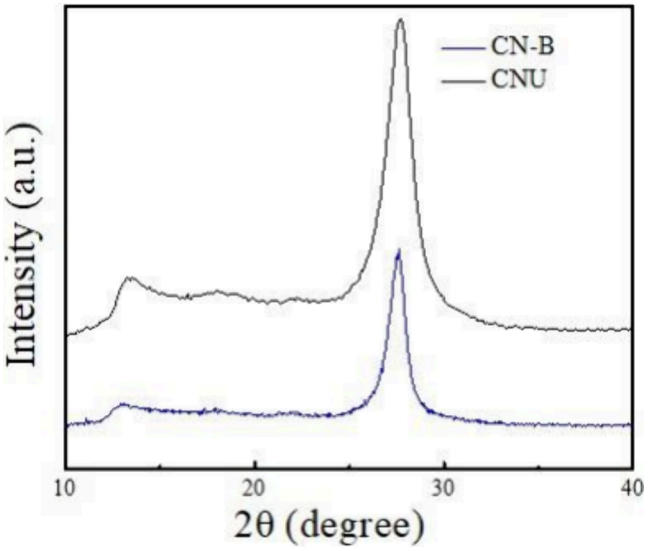

Figure 2. XRD patterns of bulk g-C_3N_4 (CN-B) and CNU.

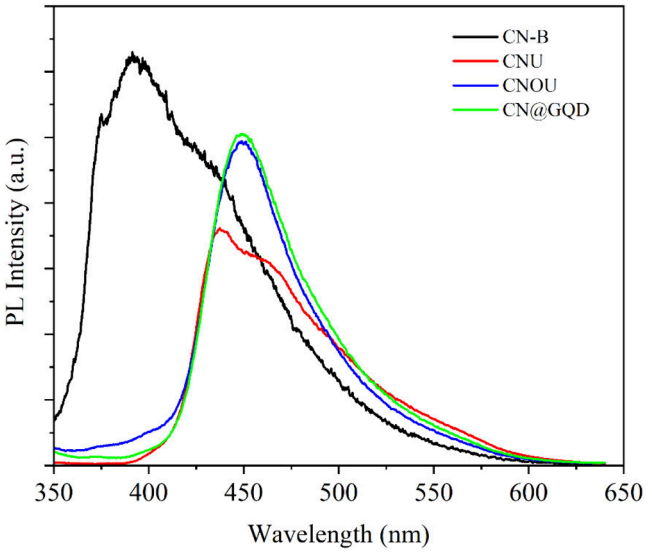

Figure 4. PL spectra of prepared GCN photocatalysts.

to promote electron−hole pair formation by supplying photons with sufficient energy.[33] Nevertheless, the band gap of CNU (3.02 eV) was the highest, while CN-B has the smallest band gap among the catalysts studied (Figure 3b).

Although CNU has the largest band gap among the as-synthesized catalysts, it achieved the lowest photoluminescence (PL) emission upon UV light irradiation (Figure 4). In contrast, while having a smaller band gap, CN-B and CNOU have a higher PL intensity. Hence, it was evidenced that CNU has a lower charge recombination rate than CN-B, CNOU, and CN@GQD.

3.2. Photocatalytic Activities of the GCNs. To evaluate the photocatalytic activities of the as-prepared GCN, a series of photocatalytic TC degradation reactions were performed with and without the photocatalysts. As depicted in Figure 5, the control test demonstrated that the concentration of TC does not change in the dark conditions. Under visible light irradiation, TC experiences only a very small extent of degradation without the presence of photocatalysts. In contrast, the concentration of TC solutions mixed with as-prepared GCN catalysts declined between 1.7%−8.4% during the adsorption−desorption equilibrium process. It is observed that only 60.4% of TC was degraded by CN-B after 60 min of the photocatalytic degradation reaction. Enhanced photo-

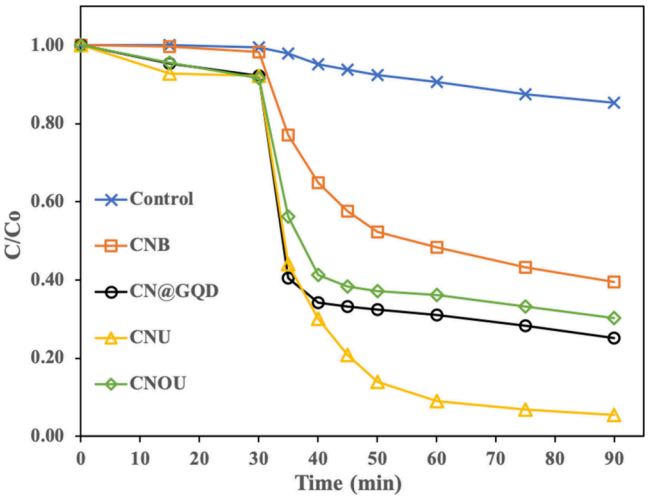

Figure 5. Removal of TC with different photocatalysts under visible light irradiation (500 mg/L photocatalysts, pH 7, and 25 ppm TC). The control test was performed under the same conditions but without a catalyst.

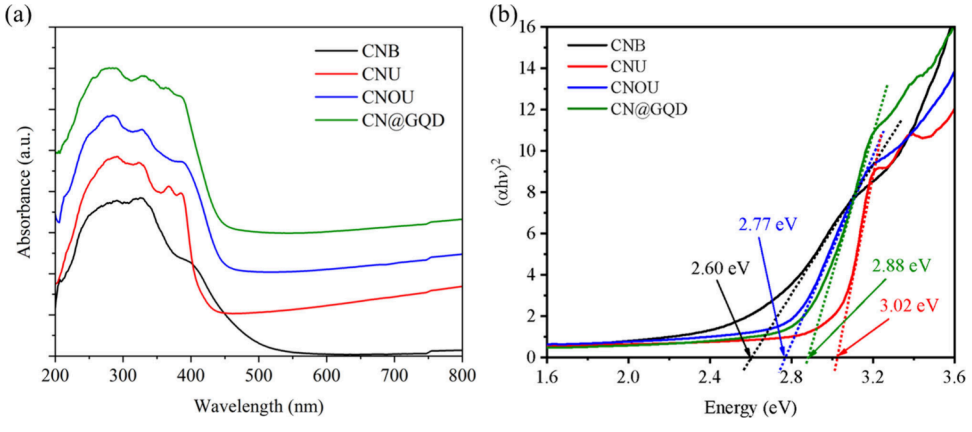

Figure 3. (a) The UV−vis DRS spectra and (b) Tauc plot of CN-B, CNU, CNOU, and CN@GQD.

https://doi.org/10.1021/acsagscitech.4c00637
ACS Agric. Sci. Technol. XXXX, XXX, XXX−XXX

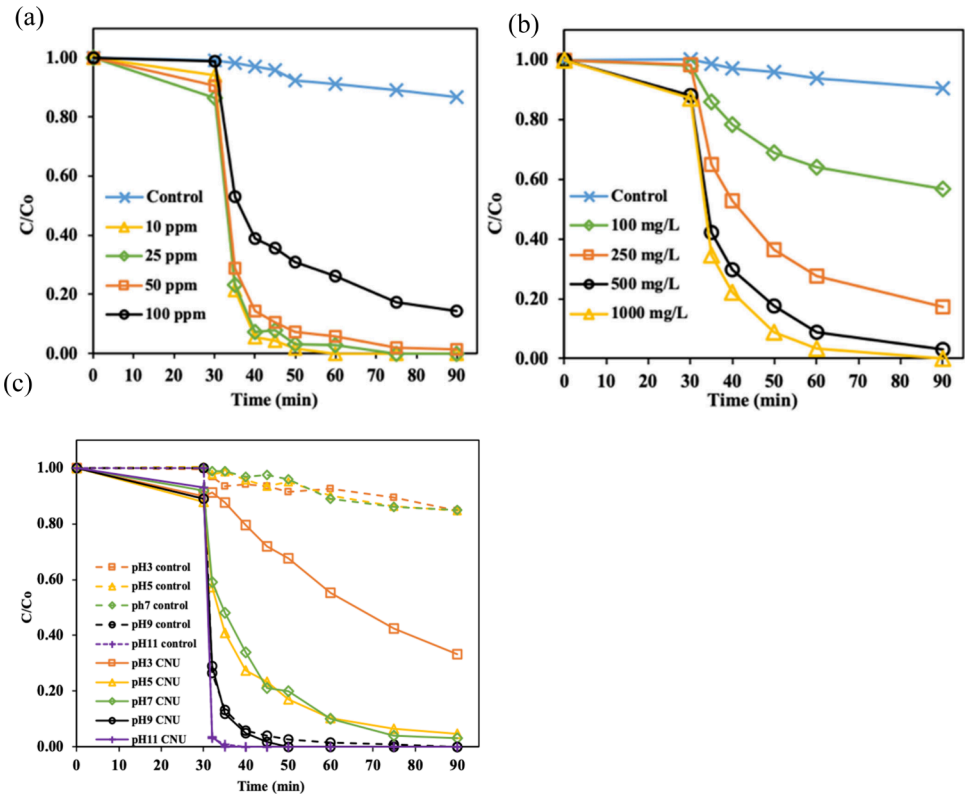

Figure 6. Removal of TC at different (a) CNU dosages, (b) initial TC concentration, and (c) initial pH values under visible light irradiation. The control tests were conducted without addition of catalyst.

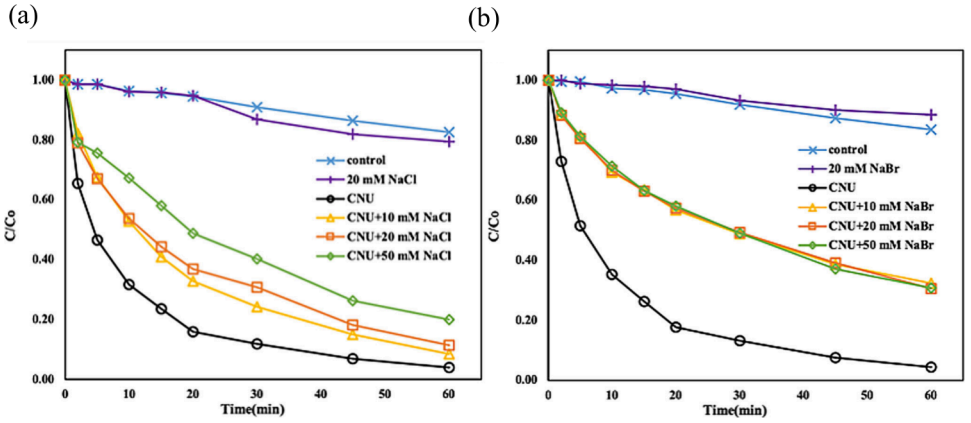

Figure 7. Photodegradation of TC with different amounts of (a) NaCl and (b) NaBr under visible light irradiation.

catalytic TC degradation was recorded at 69.7% and 74.9% when CNOU and CN@GQD were added, respectively. CNU, which degrades 94.4% of TC after 60 min under visible light, has the highest activity among the four catalysts. Due to its superior photocatalytic performance and energy efficiency, CNU is selected for subsequent experiments to explore the influence of different reaction conditions on its photocatalytic activity.

3.3. Influence of Reaction Conditions. Several experiments were performed to elucidate the influence of the reaction conditions on the photocatalytic activity of CNU. Figure 6a shows the effect of the CNU dosage on degrading 25 ppm of TC under visible light. As the doses of CNU increased from 100 mg/L to 1000 mg/L, the efficiency of photodegradation increased. This improvement in TC degradation is ascribed to the increasing number of active sites with increasing amounts of photocatalysts. Eventually, total removal of TC can be achieved within 90 min of reaction when 1000 mg/L of CNU was applied. Figure 6b displays the trend in the photodegradation efficiency with respect to the initial TC concentration. When the initial concentration was raised from 10 to 50 ppm, more than 90% of TC was degraded after 60 min of irradiation. The photodegradation rate decreased to below 90% when the initial TC concentration was 100 ppm. At this concentration, the pollutant may occupy limited amounts of active sites on the surface of CNU, which causes a decrease in its photodegradation efficiency.

To show the efficiency of photodegradation under different pH values, NaOH and HCl were used to adjust the initial pH. As shown in Figure 6c, TC degradation was limited to below

https://doi.org/10.1021/acsagscitech.4c00637
ACS Agric. Sci. Technol. XXXX, XXX, XXX−XXX

20% in the absence of photocatalysts. The addition of CNU boosts the photodegradation rate of TC at pH 3, 5, and 7 to 66.7%, 95.2%, and 97.0%, respectively. It is observed that degradation efficiency is the highest when the solution is neutral or slightly acidic. When pH > 9, total removal of TC was achieved with and without the presence of CNU. The increase of OH^- concentration at pH > 9 will enhance the alkaline photolysis of TC at λ = 420 nm without the need for a photocatalyst, which is consistent with the previous report.[34] However, since the pH value of the surface water system is about 6−7, TC will remain stable in the environment without the addition of photocatalysts. Therefore, CNU can be an effective photocatalyst in removing TC from contaminated water.

Due to the presence of ions in surface wastewater, it is worth exploring the effect of electrolytes such as NaCl and NaBr on the photodegradation efficiency of TC. The results in Figure 7 show the types of electrolytes and water salinity are both influential on the photodegradation of TC. All the samples reach adsorption−desorption equilibrium in the dark within 30 min with negligible adsorption of TC. The photodegradation efficiency of CNU in NaCl added sample experienced a smaller extent of decrease (Figure 7a) compared to NaBr (Figure 7b). When 10 to 50 mM NaCl was introduced, the photodegradation of TC dropped to 91.7%, 88.5%, and 80.0%, respectively. This observation is ascribed to the addition of Cl^- ions, which causes the photocatalyst to aggregate into larger particles with a reduced specific surface area and the number of active sites in the solution.[35] A greater inhibitory effect was observed when NaBr was added (Figure 7b). The degradation percentage decreased to about 72% when adding 10, 20, and 50 mM of NaBr. This could be rationalized as the larger Br^- anions can block a larger area of the photocatalyst surface and effectively restrict access to active sites. To summarize, the presence of NaCl and NaBr in TC-polluted water can inhibit the process of photodegradation.

Further evaluation has been carried out on the performance of CNU in different types of water. It was shown that the photocatalytic activities of CNU in both tap water (126 μS/cm)[36] and river water (173 μS/cm)[37] were lower than it was in the ddW (<5 μS/cm) (Figure 8). This is consistent with the finding above, where the presence of ionic salts can deteriorate CNU performance. Nevertheless, the rate of TC degradation in tap water is slightly lower than in river water, which could be attributed to the complex composition of river water that contains dissolved organic matter that helped to enhance the photocatalytic degradation process. Together with findings in the study on the effect of salts, it was suggested that a low salt content water condition is required for the optimal performance of the CNU photocatalyst. This can be achieved by carrying out reverse osmosis to reduce the salt content prior to the photocatalytic water treatment process.

The photocatalytic activity of as-synthesized CNU in TC removal was compared with a number of recently reported catalysts (Table 1). It was shown that CNU has a higher reaction rate than the modified carbon nitrides (CN) and metal containing photocatalysts. Complete degradation of tetracycline was achieved in 1 h using a relatively lower power single wavelength light source, which demonstrated that CNU could be a promising photocatalyst for environment remediation.

3.4. Kinetic Study of TC Photodegradation. The reaction kinetics of photocatalytic TC degradation was fitted

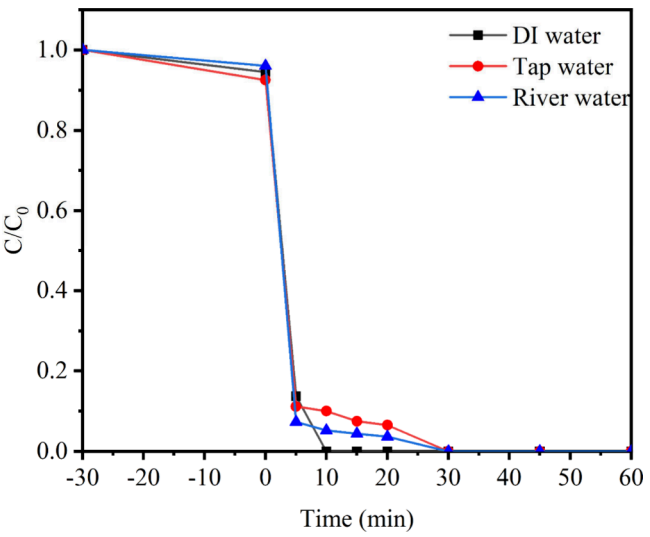

Figure 8. Effect of water chemistry on the photocatalytic degradation of TC using a CNU catalyst under visible light irradiation (500 mg/L photocatalysts, pH 7, and 25 ppm TC).

with various kinetic models (eqs 1−3). It was evidenced that CNU catalyzed photodegradation of TC was not following the Langmuir−Hinshelwood mechanism. The reaction was shown to be best fitted with the pseudo-second-order kinetic model, and hence, all experiments were fitted into the pseudo-second-order kinetic model for further analysis (Table S1).[38] The rate constants under different reaction conditions were determined and summarized in Table 2.

$$\text{Langmuir–Hinshelwood: } \frac{-t}{C - C_0} = \frac{1}{k} + \frac{1}{kK}\left[\frac{\ln(C - C_0)}{C - C_0}\right] \quad (1)$$

$$\text{Pseudo-first-order: } \ln\frac{C}{C_0} = kt \quad (2)$$

$$\text{Pseudo-second-order: } \frac{1}{C} - \frac{1}{C_0} = kt \quad (3)$$

whereas C is the TC concentration (mg/L) at the end of the reaction, C_0 is the initial TC concentration (mg/L), k is the rate constant (min^{-1}), and t is the reaction time (min).

Among the four GCN photocatalysts studied, CNU showed the highest reaction rate constant (k = 11.7 × 10^{-3} min^{-1}), which was five to ten times the rate constant of CN-B, CNOU, and CN@GQD (1.1 × 10^{-3}, 1.9 × 10^{-3}, and 2.4 × 10^{-3} min^{-1}). The influence of CNU dosage was reflected by a 37.5-fold increase in the rate constant from 8.0 × 10^{-4} min^{-1} to 30.0 × 10^{-3} min^{-1} following an increase in the CNU dosage from 100 to 1000 mg/L. On the contrary, a higher initial TC concentration would slow down the reaction, as indicated by a decrease in the rate constant from 238.4 × 10^{-3} min^{-1} to 1.1 × 10^{-3} min^{-1} when the initial TC concentration was increased from 10 to 100 ppm. It was observed that the reaction rate increased with the initial pH. At pH 7, the rate constant was determined to be 18.9 × 10^{-3} min^{-1}. This is supported by a higher TC adsorption by CNU (Figure 5), which has a zeta potential of 6.07 and hence a slightly negatively charged surface at pH 7 (Figure S1). The negatively charged surface

https://doi.org/10.1021/acsagscitech.4c00637
ACS Agric. Sci. Technol. XXXX, XXX, XXX−XXX

Table 1. Photocatalytic TC Degradation Performance of Various Catalysts

catalyst	light wavelength (nm)	light power (W)	catalyst dosage (mg/L)	TC concentration (ppm)	reaction time (h)	removal rate (%)	rate constant, k ($\times 10^{-3}$ min^{-1})	reference
CNU	420	100	500	10	1	100	238.4	This study
OPACN hydrogel	Visible	250	3000	10	0.5	88	65.4	46
FCN-5	>420	300	500	10	1	95.1	47.5	47
CN-3	>420	-	500	20	0.5	94.0	105.0	48
π-COF	Visible	300	200	20	1.5	94.8	84.6	49
BCNNT	Visible	300	250	20	0.5	80	54.9	50
Bi/NH_2-UiO-66	>420	300	200	20	2	95.8	28.0	51
CdS@V-$ZnIn_2S_4$	420	300	300	10	2	98.7	30.8	52
g-C_3N_4/BiOI	410–760	30	500	30	1	93.0	38.9	53

Table 2. Rate Constant of TC Photodegradation with Different Independent Variables

catalysts	k ($\times 10^{-3}$ min^{-1})	dosage	k ($\times 10^{-3}$ min^{-1})
CN-B	1.1	100 mg/L	0.8
CN@GQD	2.4	250 mg/L	3.5
CNU	11.7	500 mg/L	11.9
CNOU	1.9	1000 mg/L	30.0
[TC]	k ($\times 10^{-3}$ min^{-1})	pH	k ($\times 10^{-3}$ min^{-1})
10 ppm	238.4	3	1.1
25 ppm	48.2	5	12.5
50 ppm	11.3	7	18.9
100 ppm	1.1		
[NaCl]	k ($\times 10^{-3}$ min^{-1})	[NaBr]	k ($\times 10^{-3}$ min^{-1})
0 mM	9.9	0 mM	9.6
10 mM	4.1	10 mM	1.7
20 mM	3.2	20 mM	1.6
50 mM	2.0	50 mM	1.6

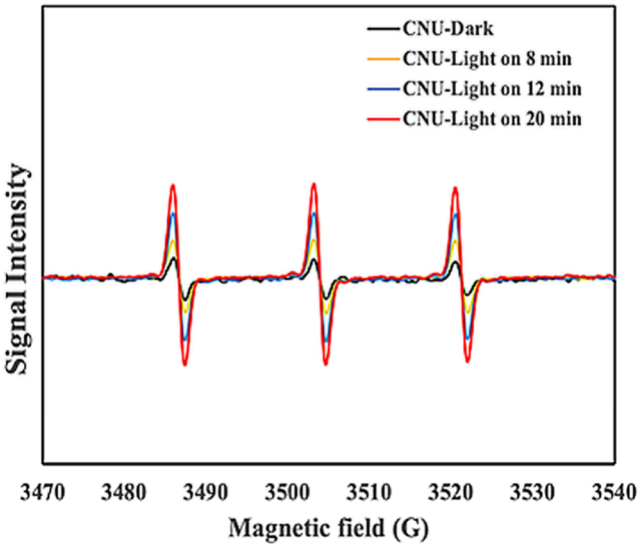

Figure 9. EPR spectra of $^1O_2$ radical trapped by TEMP in the CNU photocatalyst.

can interact better with the hydroxyl and amino groups of TC, allowing the photodegradation process to be carried out more effectively. Beyond pH 7, the rate of reaction will be greatly enhanced by the alkaline-assisted photolysis process.[39] Thus, we are unable to compare their rate constants with those measured at pH ≤ 7. The additions of NaCl and NaBr were both detrimental to the reaction kinetics of photocatalytic TC degradation. Nevertheless, the effect of adding NaCl was moderate, with the reaction rate gradually decreasing with an increasing amount of NaCl. In contrast, the addition of NaBr caused an abrupt drop in k from 9.6 × 10^{-3} min^{-1} to less than 1.6 × 10^{-3} min^{-1}.

3.5. ROS Production and Proposed Reaction Mechanism. To verify the formation of reactive oxygen species, the ESR technique was applied, and its results are depicted in Figure 9. Before measurement, as-prepared catalysts were added into ddH_2O and mixed homogeneously to simulate the reaction system of photodegradation for tetracycline. A weak signal was observed before visible light irradiation due to the formation of the TEMP spin trap product with existing singlet oxygen ($^1O_2$). Upon visible light irradiation, the ESR signal intensity of TEMP-$^1O_2$ increases along with the duration of irradiation, which indicates that the concentration of $^1O_2$ continues to increase during the reaction.[40] The generation of $^1O_2$ implies the presence of superoxide, $\bullet O_2^-$, which was a precursor to the formation of $^1O_2$ via superoxide oxidation by holes ($\bullet O_2^- + h^+ \rightarrow {}^1O_2$).[41] The formation of $\bullet O_2^-$ is a result of O_2 reduction by photogenerated electrons. Upon excitation by visible light, the electrons at the valence band of the CNU will be promoted to the conduction band and form an electron–hole pair (eq 4). These electrons at the conduction band will then reduce O_2 in the water system to form reactive $\bullet O_2^-$ molecules (eq 5), which subsequently abstract hydrogen from water molecules to produce hydroxyl (•OH) and hydroperoxyl (•OOH) radicals (eq 7). •OOH can further react with water to produce more •OH (eq 8). All $\bullet O_2^-$, •OH, and $^1O_2$ are the ROS that are responsible for oxidizing TC and degrading it to smaller molecules.

$$CNU + h\nu \rightarrow CNU + h^+(VB) + e^-(CB) \quad (4)$$

$$e^-(CB) + O_2 \rightarrow \bullet O_2^- \quad (5)$$

$$\bullet O_2^- + h^+ \rightarrow {}^1O_2 \quad (6)$$

$$\bullet O_2^- + H_2O \rightarrow \bullet OOH + \bullet OH \quad (7)$$

$$\bullet OOH + H_2O \rightarrow H_2O_2 + \bullet OH \quad (8)$$

$$2 \bullet OH \rightleftharpoons H_2O_2 \quad (9)$$

The formation of superoxides and holes was proven by a scavenging test. t-BuOH, FFA, ascorbic acid, EDTA-2Na, and

https://doi.org/10.1021/acsagscitech.4c00637
ACS Agric. Sci. Technol. XXXX, XXX, XXX–XXX

$KBrO_3$ were used as scavengers to hydroxyl radical, singlet oxygen, superoxides, holes, and electron, respectively. In Figure 10, it was depicted that the degradation rate decreased in the presence of ascorbic acid and EDTA-2Na, which evidences the reaction between superoxides and photogenerated holes to form singlet oxygen. The unobservable singlet oxygen inhibiting effect by FFA was due to the fact that TC could still be degraded by unreacted superoxides and holes. Interestingly, the addition of hydroxyl radicals and electrons scavengers enhanced the photocatalytic degradation of TC. This could be due to the formation of more hydroxyl radicals by shifting eq 9 to the left, allowing more hydroxyl radical species to participate in degrading TC. Meanwhile, electron scavenging helped to minimize the recombination of photogenerated conduction band electrons and holes and subsequently accelerated photocatalytic TC degradation.[42] The importance of superoxides and photogenerated holes was supported by the observation in section 3.3, where the presence of Cl^- and Br^- salts effectively decreased the degradation rate of TC. This inhibitory effect was attributed to the ability of these halide ions to react with both hole-induced hydroxyl radicals and superoxides.[43]

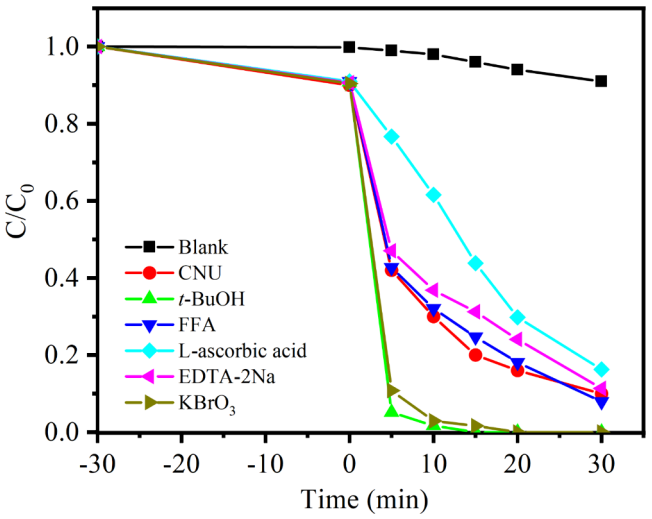

Figure 10. Photodegradation of TC with different radical scavengers (500 mg/L photocatalysts, pH 7, and 25 ppm TC).

To clarify the possible photocatalytic mechanism, LC-QTOF-MS was employed to identify the intermediates formed during the photodegradation process (Figure S2). Based on the MS spectrum, it was shown that the photodegradation reaction started with the N-demethylation of deprotonated (m/z = 443) to form Intermediate 1 (TP1, m/z = 416, Figure 11), a process that has also been previously reported during the degradation of tetracycline in a schorl/H_2O_2 system.[44] It was followed by deamination at C2[45] and dehydroxylation at C3 to produce Intermediate 2 (TP2, m/z = 387). Further degradation removed a hydroxymethyl group at C2 and a methyl group at C11 from Intermediate 2 to form Intermediate 3 (TP3, m/z = 343). Subsequent reactions caused Intermediate 3 to lose its amine group and experience dehydration at C1 and C6. Meanwhile, the double bond at C2 and C3 underwent hydroformylation and produced Intermediate 4 (TP4, m/z = 275). Next, a ring-opening reaction occurred together with the departure of an aldehyde group from Intermediate 4 to form Intermediate 5 (TP5, m/z = 217). Finally, the intermediate species continued to react with ROS to form lighter molecular weight molecules such as 1-tetralone (TP6, m/z = 141) and 3-formyl propanoic acid (TP7, m/z = 101). The CNU-catalyzed photodegradation of TC is illustrated in Figure 12.

The toxicity of TC and its degradation products was simulated, and the results are displayed in Table 3 and Figure S3. Based on the results of predictive model, it was shown that the TP5 product is toxic in the short and long term to all species, but it became very toxic toward fish and daphnia when exposed in the long term. TP3 and TP7 are particularly harmful and toxic to daphnia, while TP6 is toxic to both aquatic flora and fauna for prolonged exposure. Although they seem harmful from the computational prediction, the real risk could not be high since these trace amounts of intermediates could be further photodegraded during the reactions. The simulation has indicated that TP1, 2, and 4 are nontoxic to living organisms in water.

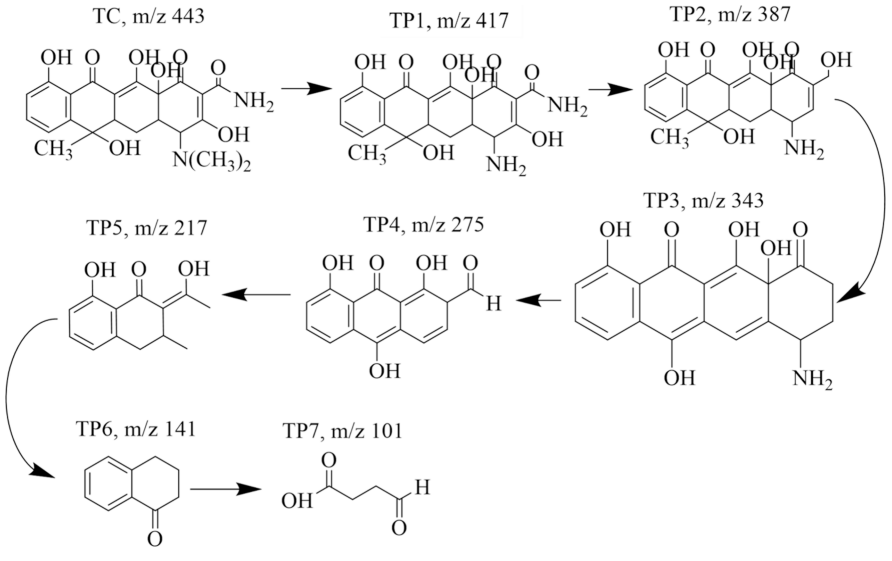

Figure 11. Proposed possible pathway of photocatalytic TC degradation in the presence of CNU.

https://doi.org/10.1021/acsagscitech.4c00637
ACS Agric. Sci. Technol. XXXX, XXX, XXX−XXX

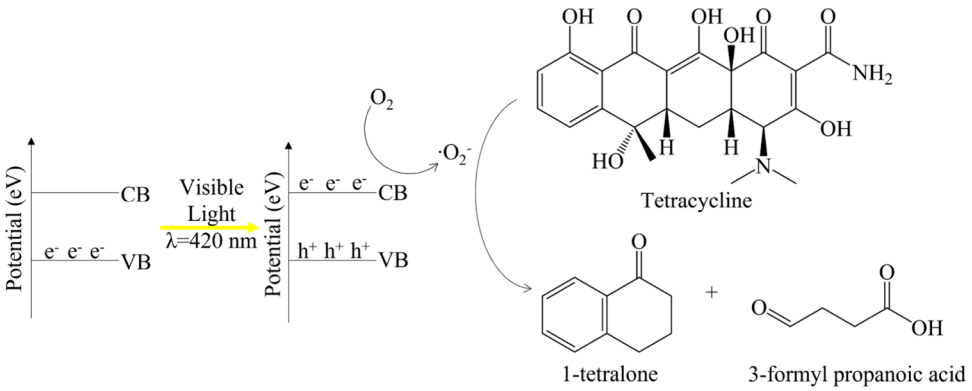

Figure 12. Reaction mechanism of CNU catalyzed photodegradation of TC (VB: Valence Band; CB: Conduction Band).

Table 3. Toxicity Prediction for TC and Its Degradation Byproducts Using the ECOSAR Tool[a]

Degradation products	Acute toxicity			Chronic toxicity		
	Fish	Daphnia	Green Algae	Fish	Daphnia	Green Algae
	96-hr LC_{50} (mg/L)	48-hr LC_{50} (mg/L)	96-hr EC_{50} (mg/L)	ChV (mg/L)	ChV (mg/L)	ChV (mg/L)
TC	13100	1060	1890	2490	59.9	474
TP1	34300	2560	5310	8250	134	1260
TP2	7790	650	1.090	1350	37.7	279
TP3	1830	169	232	233	10.8	64.0
TP4	448	247	163	42.3	22.2	40.0
TP5	6.99	4.59	6.22	0.811	0.670	2.25
TP6	34.8	20.9	19.5	3.63	2.37	5.79
TP7	891	1020	460	422	7.23	123

[a]Very toxic: $LC_{50}/EC_{50}/ChV \leq 1$, red label; Toxic: $1 < LC_{50}/EC_{50}/ChV \leq 10$, orange label; Harmful: $10 < LC_{50}/EC_{50}/ChV \leq 100$, yellow label; Not harmful, $LC_{50}/EC_{50}/ChV > 100$, green label.

3.6. Cyclic Test. The durability and reusability of CNU were evaluated through a cyclic test which observes its performance and change in solution pH over three cycles of photocatalytic TC degradation reactions. The results showed that CNU suffered from a loss of activity with an increasing number of reactions with the removal rate reduced by approximately 40% (Figure S4). Meanwhile, the solution pH became more acidic following three cycles of the reaction. This is consistent with the proposed mechanism in which 3-formyl propanoic acid was produced as a TC degradation product. The cyclic test result indicated that CNU seems not to have good reusability, which could be due to the loss of CNU during our recycling operations that require further improvement in the future.

In summary, it is proven that preparing graphitic carbon nitride from urea is an effective method to enhance its photocatalytic activity. Urea-derived GCN has irregular, stacked microsheet structures with a smaller crystallite size. Among the four GCNs studied in this research, CNU achieved the highest photocatalytic activity in the degradation of TC. The optimum reaction condition for CNU-catalyzed photodegradation of TC is determined to be 1000 mg/L catalyst and 10 ppm initial TC concentration. The CNU photocatalyst is shown to be effective at pH 7, a pH level at which alkaline-assisted photolysis does not occur due to the absence of hydroxide ions. This study has also demonstrated that the presence of sodium halide salts has a negative impact on the photocatalytic activity of CNU. The results of the mechanistic study suggested that photoexcited electrons generated when CNU is exposed to visible light react with molecular oxygen to form reactive superoxides. Together with photogenerated holes, they are responsible for the photocatalytic degradation of TC to simpler 1-tetralone and 3-formyl propanoic acid.

■ ASSOCIATED CONTENT

Supporting Information

The Supporting Information is available free of charge at https://pubs.acs.org/doi/10.1021/acsagscitech.4c00637.

Figure S1. The zeta potential of photocatalyst CNU under different pH. Figure S2. LC-QTOF/MS analysis of TC by-products. Figure S3. Prediction of TC degradation products acute toxicity and chronic toxicity using the ECOSAR tool. Figure S4. Cyclic test of CNU. Table S1. Rate constant and R2 of photocatalytic TC degradation fit into different kinetic models (PDF)

https://doi.org/10.1021/acsagscitech.4c00637
ACS Agric. Sci. Technol. XXXX, XXX, XXX−XXX

AUTHOR INFORMATION

Corresponding Author

Yang-hsin Shih − *Department of Agricultural Chemistry, National Taiwan University, Taipei 106, Taiwan;* orcid.org/0000-0002-1326-0720; Phone: +886-2-33669442; Email: yhs@ntu.edu.tw; Fax: +886-2-33669442

Authors

Sheng-Eng Huang − *Department of Agricultural Chemistry, National Taiwan University, Taipei 106, Taiwan*

Kok-Hou Tan − *Department of Agricultural Chemistry, National Taiwan University, Taipei 106, Taiwan; Cardiff Catalysis Institute, Translational Research Hub, Cardiff University, Cardiff CF24 4HQ, U.K.;* orcid.org/0000-0002-4119-0686

Rama Shanker Sahu − *Department of Agricultural Chemistry, National Taiwan University, Taipei 106, Taiwan;* orcid.org/0000-0001-8940-4666

Tesfaye Abebe Geleta − *Department of Agricultural Chemistry, National Taiwan University, Taipei 106, Taiwan;* orcid.org/0000-0002-6972-5881

Ashkan Miri − *Department of Agricultural Chemistry, National Taiwan University, Taipei 106, Taiwan*

Chen-yu Lin − *Department of Agricultural Chemistry, National Taiwan University, Taipei 106, Taiwan*

Wen-Ling Chen − *Institute of Food Safety and Health, College of Public Health and Department of Public Health, College of Public Health, National Taiwan University, Taipei 100, Taiwan*

Complete contact information is available at: https://pubs.acs.org/10.1021/acsagscitech.4c00637

Notes

The authors declare no competing financial interest.

ACKNOWLEDGMENTS

The authors gratefully acknowledge the financial support of the National Science and Technology Council of Taiwan (No. 110-2221-E-002-132 and 109-2813-C-002-020-E). The authors would also like to express our gratitude to Ms. S.-J. Ji from the Instrumentation Center of National Taiwan University (NTU), which is supported by the National Science and Technology Council, Taiwan, for assistance in SEM measurements, to Prof. H. M. Chen for DRS at Department of Chemistry in NTU, to Prof. M. H. Li for PL at Department of Geography in NTU, and to H. -N. Huang for EPR at National Taiwan Normal University Instrumentation Center.

REFERENCES

(1) Xu, L.; Zhang, H.; Xiong, P.; Zhu, Q.; Liao, C.; Jiang, G. Occurrence, Fate, and Risk Assessment of Typical Tetracycline Antibiotics in the Aquatic Environment: A Review. *Sci. Total Environ.* **2021**, *753*, 141975.

(2) Aalipour, F.; Mirlohi, M.; Jalali, M.; Azadbakht, L. Dietary Exposure to Tetracycline Residues through Milk Consumption in Iran. *J. Environ. Health Sci. Eng.* **2015**, *13* (1). DOI: 10.1186/s40201-015-0235-6.

(3) Önal, A. Overview on Liquid Chromatographic Analysis of Tetracycline Residues in Food Matrices. *Food Chem.* **2011**, *127* (1), 197.

(4) Golub, L. M.; Elburki, M. S.; Walker, C.; Ryan, M.; Sorsa, T.; Tenenbaum, H.; Goldberg, M.; Wolff, M.; Gu, Y. Non-Antibacterial Tetracycline Formulations: Host-Modulators in the Treatment of Periodontitis and Relevant Systemic Diseases. *Int. Dent J.* **2016**, *66* (3), 127.

(5) Barbieri, J. S.; Hoffstad, O.; Margolis, D. J. Duration of Oral Tetracycline-Class Antibiotic Therapy and Use of Topical Retinoids for the Treatment of Acne among General Practitioners (GP): A Retrospective Cohort Study. *J. Am. Acad. Dermatol* **2016**, *75* (6), 1142.

(6) Daghrir, R.; Drogui, P. Tetracycline Antibiotics in the Environment: A Review. *Environ. Chem. Lett.* **2013**, *11* (3), 209−227.

(7) Gothwal, R.; Shashidhar, T. Antibiotic Pollution in the Environment: A Review. *Clean (Weinh)* **2015**, *43* (4), 479.

(8) Rodriguez-Mozaz, S.; Chamorro, S.; Marti, E.; Huerta, B.; Gros, M.; Sànchez-Melsió, A.; Borrego, C. M.; Barceló, D.; Balcázar, J. L. Occurrence of Antibiotics and Antibiotic Resistance Genes in Hospital and Urban Wastewaters and Their Impact on the Receiving River. *Water Res.* **2015**, *69*, 234.

(9) Liu, J.; Zhou, B.; Zhang, H.; Ma, J.; Mu, B.; Zhang, W. A Novel Biochar Modified by Chitosan-Fe/S for Tetracycline Adsorption and Studies on Site Energy Distribution. *Bioresour. Technol.* **2019**, *294*, 122152.

(10) Huang, X.; Zhu, N.; Mao, F.; Ding, Y.; Zhang, S.; Liu, H.; Li, F.; Wu, P.; Dang, Z.; Ke, Y. Enhanced Heterogeneous Photo-Fenton Catalytic Degradation of Tetracycline over YCeO2/Fh Composites: Performance, Degradation Pathways, Fe2+ Regeneration and Mechanism. *Chemical Engineering Journal* **2020**, *392*, 123636.

(11) Yang, J.; Lin, Y.; Yang, X.; Ng, T. B.; Ye, X.; Lin, J. Degradation of Tetracycline by Immobilized Laccase and the Proposed Transformation Pathway. *J. Hazard Mater.* **2017**, *322*, 525.

(12) Wang, J.; Zhi, D.; Zhou, H.; He, X.; Zhang, D. Evaluating Tetracycline Degradation Pathway and Intermediate Toxicity during the Electrochemical Oxidation over a Ti/Ti4O7 Anode. *Water Res.* **2018**, *137*, 324.

(13) Wu, S.; Hu, H.; Lin, Y.; Zhang, J.; Hu, Y. H. Visible Light Photocatalytic Degradation of Tetracycline over TiO_2. *Chemical Engineering Journal* **2020**, *382*, 122842.

(14) Hansson, H.; Kaczala, F.; Marques, M.; Hogland, W. Photo-Fenton and Fenton Oxidation of Recalcitrant Industrial Wastewater Using Nanoscale Zero-Valent Iron. *International Journal of Photoenergy* **2012**, *2012*, 1.

(15) Shao, S.; Wu, X. Microbial Degradation of Tetracycline in the Aquatic Environment: A Review. *Crit Rev. Biotechnol* **2020**, *40* (7), 1010.

(16) Woisetschläger, D.; Humpl, B.; Koncar, M.; Siebenhofer, M. Electrochemical Oxidation of Wastewater - Opportunities and Drawbacks. *Water Sci. Technol.* **2013**, *68* (5), 1173.

(17) Liu, X.; Liu, Y.; Lu, S.; Guo, W.; Xi, B. Performance and Mechanism into TiO2/Zeolite Composites for Sulfadiazine Adsorption and Photodegradation. *Chemical Engineering Journal* **2018**, *350*, 131.

(18) Aboutaleb, W. A.; El-Salamony, R. A. Effect of Fe2O3-CeO2 Nanocomposite Synthesis Method on the Congo Red Dye Photodegradation under Visible Light Irradiation. *Mater. Chem. Phys.* **2019**, *236*, 121724.

(19) Li, P.; Cao, W.; Zhu, Y.; Teng, Q.; Peng, L.; Jiang, C.; Feng, C.; Wang, Y. NaOH-Induced Formation of 3D Flower-Sphere BiOBr/Bi4O5Br2 with Proper-Oxygen Vacancies via in-Situ Self-Template Phase Transformation Method for Antibiotic Photodegradation. *Sci. Total Environ.* **2020**, *715*, 136809.

(20) He, F.; Wang, Z.; Li, Y.; Peng, S.; Liu, B. The Nonmetal Modulation of Composition and Morphology of G-C3N4-Based Photocatalysts. *Appl. Catal., B* **2020**, *269*, 118828.

(21) Mishra, A.; Mehta, A.; Basu, S.; Shetti, N. P.; Reddy, K. R.; Aminabhavi, T. M. Graphitic Carbon Nitride (g−C3N4)−Based Metal-Free Photocatalysts for Water Splitting: A Review. *Carbon N Y* **2019**, *149*, 693.

(22) Wang, K.; Li, Q.; Liu, B.; Cheng, B.; Ho, W.; Yu, J. Sulfur-Doped g-C3N4 with Enhanced Photocatalytic CO2-Reduction Performance. *Appl. Catal., B* **2015**, *176−177*, 44.

(23) Li, G.; Nie, X.; Chen, J.; Jiang, Q.; An, T.; Wong, P. K.; Zhang, H.; Zhao, H.; Yamashita, H. Enhanced Visible-Light-Driven Photocatalytic Inactivation of Escherichia Coli Using g-C3N4/TiO2 Hybrid Photocatalyst Synthesized Using a Hydrothermal-Calcination Approach. *Water Res.* **2015**, *86*, 17.
(24) Jing, L.; Wang, D.; He, M.; Xu, Y.; Xie, M.; Song, Y.; Xu, H.; Li, H. An Efficient Broad Spectrum-Driven Carbon and Oxygen Co-Doped g-C3N4 for the Photodegradation of Endocrine Disrupting: Mechanism, Degradation Pathway, DFT Calculation and Toluene Selective Oxidation. *J. Hazard Mater.* **2021**, *401*, 123309.
(25) Chang, X.; Yao, X.; Ding, N.; Yin, X.; Zheng, Q.; Lu, S.; Shuai, D.; Sun, Y. Photocatalytic Degradation of Trihalomethanes and Haloacetonitriles on Graphitic Carbon Nitride under Visible Light Irradiation. *Sci. Total Environ.* **2019**, *682*, 200.
(26) Hu, K.; Li, R.; Ye, C.; Wang, A.; Wei, W.; Hu, D.; Qiu, R.; Yan, K. Facile Synthesis of Z-Scheme Composite of TiO_2 Nanorod/g-C3N4 Nanosheet Efficient for Photocatalytic Degradation of Ciprofloxacin. *J. Clean Prod* **2020**, *253*, 120055.
(27) Oluwole, A. O.; Olatunji, O. S. Photocatalytic Degradation of Tetracycline in Aqueous Systems under Visible Light Irridiation Using Needle-like SnO2 Nanoparticles Anchored on Exfoliated g-C3N4. *Environ. Sci. Eur.* **2022**, *34* (1). DOI: 10.1186/s12302-021-00588-7.
(28) Thi Quyen, V.; Jae Kim, H.; Kim, J. T.; Thi Thu Ha, L.; Thi Huong, P.; My Thanh, D.; Minh Viet, N.; Quang Thang, P. Synthesizing S-Doped Graphitic Carbon Nitride for Improvement Photodegradation of Tetracycline under Solar Light. *Sol. Energy* **2021**, *214*, 288.
(29) Singh, P.; Ansu, A. K.; Sharma, R. K.; Goyal, R. Urea-Derived Graphitic Carbon Nitride/Polyethylene Glycol Form-Stable Composite for Thermal Energy Storage. *Energy Fuels* **2023**, *37* (5), 4058.
(30) Sahu, R. S.; Shih, Y.-h.; Chen, W.-L. New Insights of Metal Free 2D Graphitic Carbon Nitride for Photocatalytic Degradation of Bisphenol A. *J. Hazard Mater.* **2021**, *402*, 123509.
(31) Liu, H.; Qu, J.; Zhang, T.; Ren, M.; Zhang, Z.; Cheng, F.; He, D.; Zhang, Y.-n. Insights into Degradation Pathways and Toxicity Changes during Electro-Catalytic Degradation of Tetracycline Hydrochloride. *Environ. Pollut.* **2020**, *258*, 113702.
(32) Qin, J.; Wang, S.; Ren, H.; Hou, Y.; Wang, X. Photocatalytic Reduction of CO_2 by Graphitic Carbon Nitride Polymers Derived from Urea and Barbituric Acid. *Appl. Catal., B* **2015**, *179*, 1.
(33) Muhammad, W.; Khan, A.; Hussain, S.; Khan, H.; Abumousa, R. A.; Bououdina, M.; Khan, I.; Iqbal, S.; Humayun, M. Enhanced Light Absorption and Charge Carrier's Separation in g-C3N4-Based Double Z-Scheme Heterostructure Photocatalyst for Efficient Degradation of Navy-Blue Dye. *Green Chem. Lett. Rev.* **2024**, *17* (1). DOI: 10.1080/17518253.2024.2381591.
(34) Mohammed-Ali, M. A. J. Stability Study of Tetracycline Drug in Acidic and Alkaline Solutions by Colorimetric Method. *J. Chem. Pharm. Res.* **2012**, *4* (2), 1319−1326.
(35) Shih, Y.-h.; Lin, C.-h. Effect of Particle Size of Titanium Dioxide Nanoparticle Aggregates on the Degradation of One Azo Dye. *Environmental Science and Pollution Research* **2012**, *19* (5), 1652.
(36) *Water Purification Plant Water Quality Data*; Taiwan Water Corporation**2024**.
(37) *Reservoir Water Quality Monitoring - Shihmen Reservoir*; Taiwan Ministry of Environment**2024**.
(38) Tran, H. D.; Nguyen, D. Q.; Do, P. T.; Tran, U. N. P. Kinetics of Photocatalytic Degradation of Organic Compounds: A Mini-Review and New Approach. *RSC Advances.* **2023**, *13*, 16915.
(39) Song, C.; Liu, H. Y.; Guo, S.; Wang, S. G. Photolysis Mechanisms of Tetracycline under UV Irradiation in Simulated Aquatic Environment Surrounding Limestone. *Chemosphere* **2020**, *244*, 125582.
(40) Ma, L.; Li, Z.; Jiang, Z.; Wu, X.; Chang, S.; Carabineiro, S. A. C.; Lv, K. Effect of Precursors on the Structure and Photocatalytic Performance of G-C3N4 for NO Oxidation and CO2 Reduction. *Chinese Journal of Structural Chemistry* **2024**, *43*, No. 100416.
(41) Daimon, T.; Hirakawa, T.; Kitazawa, M.; Suetake, J.; Nosaka, Y. Formation of Singlet Molecular Oxygen Associated with the Formation of Superoxide Radicals in Aqueous Suspensions of TiO2 Photocatalysts. *Appl. Catal. A Gen* **2008**, *340* (2), 169.
(42) El-Morsi, T. M.; Budakowski, W. R.; Abd-El-Aziz, A. S.; Friesen, K. J. Photocatalytic Degradation of 1,10-Dichlorodecane in Aqueous Suspensions of TiO2: A Reaction of Adsorbed Chlorinated Alkane with Surface Hydroxyl Radicals. *Environ. Sci. Technol.* **2000**, *34* (6), 1018.
(43) Bragetta, M.; Germani, R.; Tiecco, M.; Alabed, H. B. R.; Del Giacco, T. Effect of Halide Ions on the TiO_2-Mediated Photocatalysis of Carbendazim in Aqueous Medium Under Near-Ultraviolet Light Irradiation. *Water Air Soil Pollut* **2024**, *235* (11). DOI: 10.1007/s11270-024-07523-5.
(44) Zhang, Y.; Shi, J.; Xu, Z.; Chen, Y.; Song, D. Degradation of Tetracycline in a Schorl/H_2O_2 System: Proposed Mechanism and Intermediates. *Chemosphere* **2018**, *202*, 661.
(45) Chen, X.; Yang, Y.; Ke, Y.; Chen, C.; Xie, S. A Comprehensive Review on Biodegradation of Tetracyclines: Current Research Progress and Prospect. *Sci. Total Environ.* **2022**, *814*, 152852.
(46) Balakrishnan, A.; Chinthala, M.; Kumar, A.; Rtimi, S. Construction of Dual Z-Scheme Ternary Carbon Nitride Homojunction Pectin Microspheres as a Multifunctional Photocatalyst for Tetracycline Degradation, H2O2 Production, and N2 Fixation. *Chemical Engineering Journal* **2024**, *496*, 153899.
(47) Zhou, Y.; Jiang, D.; Wang, Z.; Yi, L.; Sun, J.; Liu, D.; Yu, X.; Chen, Y. Bandgap Engineering of Carbon Nitride by Formic Acid Assisted Thermal Treatment for Photocatalytic Degradation of Tetracycline Hydrochloride. *Chemical Engineering Journal* **2024**, *485*, 149830.
(48) Jiang, L.; He, Z.; Jiang, T.; Hu, Y.; Wei, H.; Hong, P.; Yuan, M.; You, Y.; Yang, P.; Ma, Z.; Liang, C. Sustainable Photodegradation of Tetracycline by Surface-Functionalized Carbon Nitride: Mechanism Insight and Toxicity Assessment. *Colloids Surf. A Physicochem Eng. Asp* **2025**, *705*, 135612.
(49) Hu, Z.; Wang, Y.; Wang, L.; Wang, Q.; Zhang, Q.; Cui, F.; Jiang, G. Synthesis of S-Type Heterostructure π-COF for Photocatalytic Tetracycline Degradation. *Chemical Engineering Journal* **2024**, *479*, 147534.
(50) Wen, S.; Tang, X.; Zhou, G.; Song, J.; Ma, R.; Mao, G.; Zhang, L.; Yin, J.; Ang, E. H. Gas-Phase Self-Assembly: Converting 2D Graphitic Carbon Nitride into 1D Nanotubes for Improved Photocatalytic Tetracycline Degradation. *Ceram. Int.* **2024**, *50* (9), 14686.
(51) Jing, S.; Wang, H.; Wang, A.; Cheng, R.; Liang, H.; Chen, F.; Brouzgou, A.; Tsiakaras, P. Surface Plasmon Resonance Bismuth-Modified NH2-UiO-66 with Enhanced Photocatalytic Tetracycline Degradation Performance. *J. Colloid Interface Sci.* **2024**, *655*, 120.
(52) Almajidi, Y. Q.; Al-dolaimy, F.; Alsaab, H. O.; Althomali, R. H.; Jabbar, H. S.; Abdullaev, S. S.; Hassan, Z. F.; Ridha, B. M.; Alsalamy, A. H.; Akram, S. V. Build-in Internal Electric Field in Vacancy Engineered CdS@ZnIn2S4 Type-II Heterostructure for Boosting Photocatalytic Tetracycline Degradation and in-Situ H_2O_2 Generation. *Mater. Res. Bull.* **2024**, *170*, 112570.
(53) Kuate, L. J. N.; Chen, Z.; Yan, Y.; Lu, J.; Guo, F.; Wen, H.; Shi, W. Construction of 2D/3D Black g-C3N4/BiOI S-Scheme Heterojunction for Boosted Photothermal-Assisted Photocatalytic Tetracycline Degradation in Seawater. *Mater. Res. Bull.* **2024**, *175*, 112776.

https://doi.org/10.1021/acsagscitech.4c00637
ACS Agric. Sci. Technol. XXXX, XXX, XXX−XXX